Electronic structure of oxygen-vacancy defects in amorphous In-Ga-Zn-O semiconductors

Hyeon-Kyun Noh and K. J. Chang[*]
Department of Physics, Korea Advanced Institute of Science and Technology, Daejeon 305-701, Korea

Byungki Ryu and Woo-Jin Lee
Samsung Advanced Institute of Technology, Yongin 446-712, Korea
(Received 24 February 2011; revised manuscript received 11 June 2011; published 15 September 2011)

We perform first-principles density functional calculations to investigate the atomic and electronic properties of various O-vacancy (V_O) defects in amorphous indium gallium zinc oxides (*a*-IGZO). The formation energies of V_O have a tendency to increase with increasing number of neighboring Ga atoms, whereas they are generally low in the environment surrounded with In atoms. Thus, adding Ga atoms suppresses the formation of O-deficiency defects, which are considered as the origin of device instability in *a*-IGZO-based thin film transistors. The conduction band edge state is characterized by the In *s* orbital and insensitive to disorder, in good agreement with the experimental finding that increasing the In content enhances the carrier density and mobility. In *a*-IGZO, while most V_O defects are deep donors, some of the defects act as shallow donors due to local environments different from those in crystalline oxides. As ionized O vacancies can capture electrons, it is suggested that these defects are responsible for positive shifts of the threshold voltage observed under positive gate bias stress. Under light illumination stress, V_O defects can be ionized, becoming V_O^{2+} defects due to the negative-*U* behavior. When electrons are captured by applying a negative bias voltage, ionized V_O^{2+} defects return to the original neutral charge state. Through molecular dynamics simulations, we find that the initial neutral state is restored by annealing, in good agreement with experiments, although the annealing temperature depends on the local environment. Our calculations show that V_O defects play an important role in the instability of *a*-IGZO-based devices.

DOI: 10.1103/PhysRevB.84.115205 PACS number(s): 71.23.Cq, 71.15.Mb, 71.55.Jv, 61.72.jd

I. INTRODUCTION

Amorphous Zn-related oxide semiconductors have attracted much attention as active matrix channels in flexible thin film transistors because of the large band gaps, unintentional *n*-type conductivity, and excellent uniformity.[1,2] In particular, amorphous In-Ga-Zn-O (*a*-IGZO) has shown good characteristics as a channel material, as compared to covalently bonded amorphous Si: field-effect mobilities are significantly enhanced by more than a factor of 10 due to the In *s* orbital character in the conduction band.[2–4]

Despite many advantages, *a*-IGZO-based devices suffer from a high density of charge traps, which cause device instability under bias stress and light illumination. When a positive gate voltage is applied, the threshold voltage (V_{th}) is positively shifted, while good stability is maintained under negative gate bias stress.[5,6] Previous experiments showed that thermal annealing mitigates the device instability, which was attributed to the reduction of electron traps.[7–11] The positive V_{th} shift is very sensitive to ambient gases such as O_2 and H_2O,[12,13] and also to the gate dielectric materials.[14–16] While O-vacancy (V_O) defects and distorted In-O polyhedra were suggested to be responsible for the positive V_{th} shift,[17] the origin of the electron traps is still not clearly known.

On the other hand, when a negative gate voltage with light illumination is applied to *a*-IGZO thin film transistors, i.e., under negative bias illumination stress (NBIS), the device instability is significantly enhanced, with negative shifts of V_{th} up to −18 V.[18] The device stability is usually recovered after a long time at room temperature, and thermal annealing accelerates the recovery.[18,19] It has been suggested that the NBIS instability is caused by the charge trapping of photoinduced hole carriers.[20] First-principles density functional calculations have been performed to study the structural properties of *a*-IGZO.[21] In other theoretical calculations, the stability and electronic structure of V_O defects in *a*-IGZO have been investigated; however, the effect of V_O on the NBIS instability was not considered.[9,10] In crystalline In-Ga-Zn-O, V_O defects were shown to be deep donors.[22] Recently, we have proposed that V_O defects act as hole traps and cause the NBIS instability in *a*-IGZO devices.[23] To understand the origin of device instability in *a*-IGZO thin film transistors, a comprehensive study is still required.

In this work, we report the details of first-principles calculations for the atomic and electronic properties of various V_O defects in *a*-IGZO. For amorphous models generated through molecular dynamics simulations, we analyze the characteristics of band edge states to determine the nature of carrier conduction, and study the effects of local environments around the vacancy site on the stability, defect levels, and charge transition levels of V_O defects. Molecular dynamics simulations are also carried out to examine the effects of thermal annealing on the stability of V_O defects, which are initially ionized by light illumination and then capture electrons by applying a negative gate voltage. Finally, we discuss the role of V_O defects in the instability of *a*-IGZO thin film transistors under various stress conditions.

II. CALCULATION METHOD

Our first-principles calculations were performed within the density functional theory framework. We used the generalized gradient approximation (GGA) for the exchange-correlation

 ©2011 American Physical Society

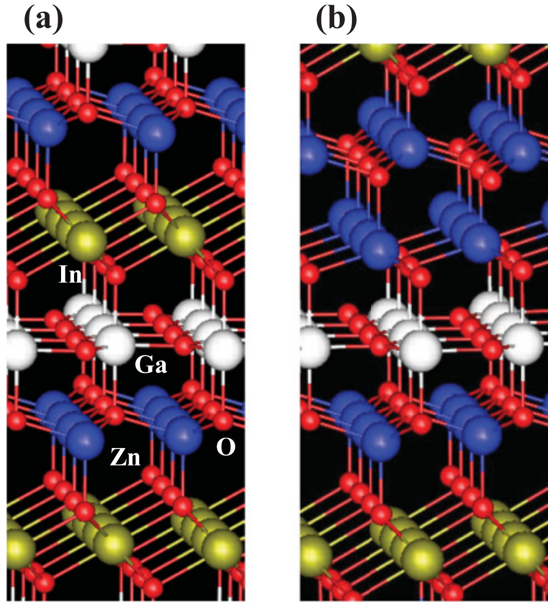

FIG. 1. (Color online) The atomic structures of $InGaO_3(ZnO)_m$ with (a) $m = 1$ and (b) $m = 3$, in which the Ga atoms form a flat boundary.

potential[24] and the projector augmented wave potentials for ionic potentials,[25] as implemented in the VASP code.[26] For a supercell containing 84 host atoms, the wave functions were expanded in plane waves. We generated three atomic models for *a*-IGZO through melt-and-quench *ab initio* molecular dynamics simulations,[27] where a canonical ensemble is realized by using a Nosé thermostat which introduces an extra degree of freedom, the Nosé mass, to control the temperature fluctuation.[28] In our calculations, the Nosé mass was chosen so that the fluctuation frequency corresponds to the maximum phonon frequency of ZnO.[29] In model 1, crystalline $InGaO_3(ZnO)_m$ (*c*-IGZO) with $m = 1$ (see Fig. 1) was melted at a temperature of 3000 K for 10 ps and then quenched rapidly at a rate of 500 K every 1.6 ps. Similarly, models 2 and 3 were obtained by using models 1 and 2 respectively as the starting configurations. For the three amorphous models, we examined the pair-correlation function and found that the 84-atom supercell is sufficient to describe the amorphous character, as in previous theoretical calculations.[21] In order to make calculations efficient, we first used a low-energy cutoff of 205 eV and only the Γ point in the Brillouin zone integration.

In the GGA calculations, the metal d bands are overestimated and the band gap is severely underestimated. The band gap is partially improved by including an on-site Coulomb correlation interaction between the localized metal d electrons, which is described by a Hubbard-like term. In the GGA + U method,[30] the on-site Coulomb correlation U lowers the position of the narrow metal d band and thereby shifts the valence band downward by reducing the p-d hybridization. However, the GGA + U method only provides a partial correction of the band gap, as noted in previous calculations.[31,32] In the GGA + U calculations, we fully optimized the supercell volume and the ionic coordinates by using a higher-energy cutoff of 400 eV and a k-point set generated by the $4 \times 4 \times 4$ Monkhorst-Pack mesh until the residual forces were less than 0.05 eV/Å. For the optimized structures, with the parameters of $U = 7.0$, 8.0, and 8.0 eV for the In 4d, Ga 3d, and Zn 3d orbitals, respectively, we reproduced the positions of the metal d bands in good agreement with experiments.[33,34] While most calculations were done within the GGA + U method, hybrid density functional calculations,[35] which give a more reliable band gap, were additionally performed to obtain more reliable defect levels of O vacancies and their formation energies. The hybrid functional assumes the following form for the exchange-correlation energy:

$$E_{\mathrm{xc}} = \alpha E_{\mathrm{x}}^{\mathrm{HF,SR}}(\omega) + (1-\alpha)E_{\mathrm{x}}^{\mathrm{GGA,SR}}(\omega) + E_{\mathrm{x}}^{\mathrm{GGA,LR}}(\omega) + E_{\mathrm{c}}^{\mathrm{GGA}}, \quad (1)$$

where α is the mixing fraction of the exact short-range Hartree-Fock exchange $E_{\mathrm{x}}^{\mathrm{HF,SR}}$, and ω is the screening parameter, which splits the exchange energy into short- and long-range components. The GGA exchange and correlation energies are denoted by $E_{\mathrm{x}}^{\mathrm{GGA}}$ and $E_{\mathrm{c}}^{\mathrm{GGA}}$, respectively. The optimized value for α is estimated to be 0.22 to obtain the measured band gap of *a*-IGZO, with the screening parameter of $\omega = 0.2$ Å^{-1}. In this case, the positions of the metal d bands are fitted to the experimental values by varying the on-site Coulomb parameters such as $U = 3.5$, 4.0, and 4.0 eV for the In, Ga, and Zn d orbitals, respectively.

The formation energy Ω of V_{O} in charge state q is expressed as

$$\Omega\left(V_{\mathrm{O}}^{q}\right) = E_{\mathrm{tot}}\left(V_{\mathrm{O}}^{q}\right) - E_{\mathrm{tot}}^{0} + \mu_{\mathrm{O}} + q\mu_{e}, \quad (2)$$

where $E_{\mathrm{tot}}(V_{\mathrm{O}})$ and E_{tot}^{0} are the total energies of supercells with and without V_{O}, respectively, μ_{O} is the O chemical potential, and μ_e is the electron chemical potential. The electron chemical potential is defined as $\mu_e = \epsilon_{\mathrm{VBM}} + E_F + \Delta V$, where E_F is the Fermi energy relative to the valence band maximum (VBM) state ϵ_{VBM} and ΔV is the correction term of the reference potential.[36] The chemical potentials μ_i (i = In, Ga, Zn, and O) are obtained from metallic In, Ga, Zn, and the O_2 molecule, respectively. From the heats of formation for *a*-IGZO, bixbyite In_2O_3, β-Ga_2O_3, and wurtzite ZnO,[22] the range of μ_{O} is estimated to be $-8.99 \leqslant \mu_{\mathrm{O}} \leqslant -4.91$ eV, where the extreme values represent the O-poor and O-rich conditions. For charged defects, we employed a jellium background which neutralizes the charged unit cell.

III. RESULTS AND DISCUSSION

A. Atomic and electronic structure of *a*-IGZO

In crystalline $InGaO_3(ZnO)_m$ (Fig. 1), the layered structure is composed of an alternating stack of an InO_2 layer and a wurtzite (Ga/Zn)-O block.[37] For both $m = 1$ and 3, the Ga atoms form a flat boundary in the (Ga/Zn)-O block which is controlled by varying the mixing ratio of the binary constituents. The In atoms are sixfold coordinated, forming the edge-sharing network of InO_6 octahedra, whereas the Ga and Zn atoms occupy trigonal bipyramidal and tetrahedral sites, respectively. Figure 2 shows the atomic structure of one of three amorphous models generated for *a*-IGZO. In the three models, we find similar structural and electronic properties such as the coordination numbers, the density of states, and

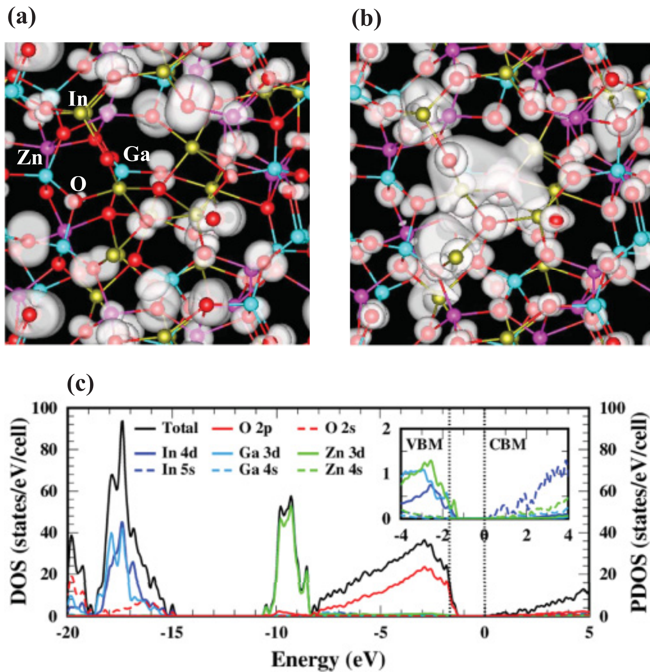

FIG. 2. (Color online) Isosurfaces of the charge densities in amorphous model 1 for a-IGZO, for (a) the localized states up to 0.34 eV above the VBM and (b) the conduction band minimum state. (c) The total density of states (DOS) and projected density of states (PDOS) onto individual atoms for the model 1, with the CBM set to zero. The inset shows the PDOS on metal atoms near the band gap.

the positions of metal d bands. The average density of a-IGZO is calculated to be about 5.58 g cm^{-3}, which is smaller by about 10% than that (6.2 g cm^{-3}) of crystalline $InGaO_3(ZnO)_m$ with $m = 1$.[21] In a-IGZO, the In, Ga, and Zn metal atoms are well distributed in the supercell, sharing the edge or vertex of their local bonding structures, which are common in amorphous systems.[38] The coordination number (N_c) of each metal atom is determined by counting the number of atoms within a sphere of the cutoff radius that is estimated from the first peak of the pair-correlation function. The average coordination numbers and average In-O, Ga-O, and Zn-O bond lengths in the GGA + U calculations are listed in Table I, and the results agree well with two extended x-ray absorption fine structure (EXAFS) measurements.[21,39] The In atoms are bonded to five or six O atoms, with the average In-O bond length of about 2.15 Å, forming the trigonal bipyramidal- or octahedral-like bonding structures. The In coordination number is estimated

TABLE I. The GGA + U results for the average coordination numbers (N_c) of the metal atoms and the average bond lengths (d) between the metal and neighboring O atoms in three amorphous modes. The cutoff radius (r_c) is determined from the first peak position of the pair-correlation function.

Metal atom	N_c	d (Å)	r_c (Å)
In	5.36 ± 0.24	2.15 ± 0.02	2.90
Ga	4.25 ± 0.18	1.79 ± 0.02	2.40
Zn	4.22 ± 0.04	2.00 ± 0.01	2.50

to be 5.36, which is smaller than that in c-IGZO. Due to the volume expansion and the loss of the layered structure, we also find changes in the Ga and Zn coordination numbers, which are estimated to be 4.25 and 4.22, respectively. Instead of trigonal bipyramidal GaO_5 clusters, tetrahedral GaO_4 clusters are mostly formed around the Ga atoms. While the Zn coordination number is slightly larger than that of wurtzite ZnO, the Zn atoms form mostly tetrahedral ZnO_4 clusters and partly trigonal bipyramidal ZnO_5 clusters. However, the local bonding structures are significantly distorted from the tetrahedral bonds, in good agreement with the Zn K-edge EXAFS analysis of the splitting of Zn-O bond lengths.[39] It is interesting to note that the Ga-O bond distance (1.79 Å) is the shortest among the three metal-O bonds. The strong Ga-O bonds indicate that the Ga atoms act as suppressors to generation of O-vacancy defects, as will be discussed later.

On the other hand, the number of metal atoms around the O atoms ranges from 2 to 4, with various composition ratios of In, Ga, and Zn atoms. The dominant composition ratios are found to be $n_{\mathrm{In}}{:}n_{\mathrm{Ga}}{:}n_{\mathrm{Zn}} = 1{:}1{:}1$, 2:1:1, and 2:1:0, which have the proportions of 15% , 13% , and 7%, respectively, where n_{In}, n_{Ga}, and n_{Zn} denote the numbers of In, Ga, and Zn atoms around the O atom. For threefold- and fourfold-coordinated O atoms, the metal-O-metal bond angles are estimated to be 95°–124°, indicating that the bonding configurations are diverse and distorted from the tetrahedral bond. In the case of twofold-coordinated O atoms, nonlinear metal-O-metal bonds are formed, reflecting the distorted local geometry.

In the GGA calculations, the metal-O bond lengths are slightly increased by about 0.1 Å, whereas the coordination numbers of metal atoms are consistent with the GGA + U calculations. The GGA + U band gaps of the three amorphous models are 1.44, 1.74, and 1.78 eV, as compared to the GGA values of 0.55, 0.71, and 0.92 eV, respectively. While the GGA + U calculations increase the band gaps due to the suppression of the p-d hybridization, the band gaps are still smaller than the bulk value of 2.51 eV for c-IGZO with $m = 1$. The smaller band gaps result from the enlarged volume and the formation of localized states near the VBM by disorders and twofold- or threefold-coordinated O atoms in the amorphous phase, while the conduction band minimum (CBM) state is not much affected. If the localized edge states are excluded, the three amorphous models have similar band gaps close to 1.78 eV. The projected densities of states onto individual atoms are drawn in Fig. 2(c). The positions of the In 4d, Ga 3d, and Zn 3d bands are located at 17.3, 17.3, and 9.5 eV below the CBM, respectively, in good agreement with the hard x-ray photoelectron spectroscopy measurements,[7] with inclusion of a band gap correction. In c-IGZO, previous calculations showed that the VBM state is characterized by the O p orbitals, with hole carriers spatially confined in the Zn-O regions.[37] In a-IGZO, we also find that the hole states are mainly composed of the O p orbitals which are hybridized with the Zn 3d orbitals. In contrast to c-IGZO, some hole states are localized near the VBM due to severely distorted and twofold- or threefold-coordinated O atoms [Fig. 2(a)]. On the other hand, there are no localized states at the CBM edge. The CBM state is composed of metal s orbitals, with a large contribution of the In s orbital [Fig. 2(b)], similar to that in c-IGZO. As the charge densities of the CBM

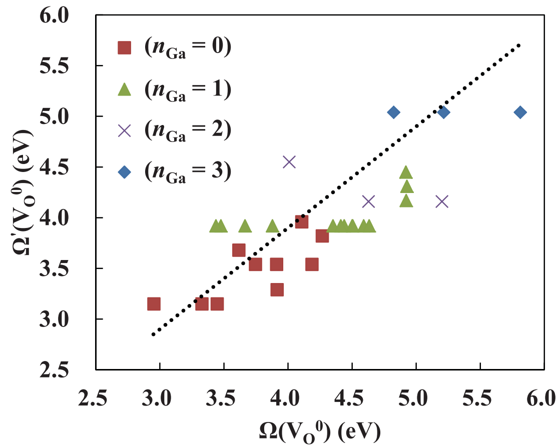

FIG. 3. (Color online) The linear fit (Ω′) of the calculated formation energies (Ω) for V_O defects in a-IGZO. The dotted line with Ω′ = Ω is drawn for guide to eye.

state are more distributed around the In atoms, electrons can move freely through the amorphous network. The absence of disorder effects on electron conduction causes high mobilities in a-IGZO-based devices.

B. O vacancy in *a*-IGZO

To investigate the electronic structure of the O vacancy, we consider 33 $V_O(n_{In}:n_{Ga}:n_{Zn})$ defects which are formed by removing the O atoms in the three amorphous models. We include 12 V_O defects with the composition ratio of $n_{In}:n_{Ga}:n_{Zn}$ = 1:1:1, which are most abundant and randomly chosen in each model. We select 8 V_O defects from three models, with the ratios of $n_{In}:n_{Ga}:n_{Zn}$ = 0:3:0, 0:0:4, 0:1:3, and 3:0:1, which also appear in c-IGZO with $m = 3$ [Fig. 1(b)], and additional 13 V_O defects with random composition ratios. For most V_O defects in the neutral state, we find that the metal atoms around the vacancy site undergo inward relaxations. Due to large relaxations up to 0.69 Å, the distances between the metal atoms are greatly reduced; thus, interactions between the metal dangling bonds are enhanced. Only four defects, including two V_O(1:1:1), one V_O(0:2:0), and one V_O(0:1:2) defects, exhibit outward relaxations, making a void around the vacancy site and thereby weakening the metal-metal bonds.

The formation energies of neutral V_O in a-IGZO, which are calculated by the GGA + U method, are plotted for different values of n_{Ga} under the extreme O-rich condition (μ_O = −4.91 eV) in Fig. 3. Depending on the local environment, the formation energies range from 2.96 to 5.82 eV, with the average energy of about 4.22 eV. As V_O is formed by breaking metal-O bonds, the formation energy is closely related to the type and number of metal atoms around the vacancy site. When the formation energies are fitted by the method of least squares,

$$\Omega'(V_O^0) = \beta_0 + \sum_{i=\mathrm{In,Ga,Zn}} \beta_i n_i, \qquad (3)$$

the coefficients are estimated to be β_0 = 2.70 eV and β_i = 0.25, 0.88, and 0.39 eV for i = In, Ga, and Zn, respectively, with the R^2 value of 0.60. It is clear that the formation energy is strongly correlated with the number of neighboring Ga atoms. As the Ga-O bond is strongest among the In-O, Ga-O, and Zn-O bonds, there is a tendency that it costs a higher energy to make an O deficiency in the environment with more Ga neighbors, as shown in Table II and Fig. 3. On the other hand, the formation energies are generally lower for V_O defects surrounded with In atoms. This result is consistent with the experimental finding that adding Ga atoms enhances the stability of a-IGZO thin film transistors, while incorporation of In atoms increases the carrier density and mobility.[40]

In c-IGZO with $m = 3$ [Fig. 1(b)], previous calculations showed that V_O is a negative-U defect, regardless of the type of neighboring metal atoms.[22] The negative-U behavior is also found for all the V_O defects considered in a-IGZO. In the +2 charge state of V_O, the neighboring metal atoms undergo outward relaxations. In many cases, where V_O is surrounded with Ga atoms, outward relaxations are significant in the amorphous network, resulting in the displacement of the vacancy site. Then, the formation energy of the +2 charge state is greatly reduced, indicating that the ionization of neutral V_O by hole capture can occur more easily in a-IGZO than in c-IGZO. For the V_O defects considered here, the results of the GGA + U and hybrid functional calculations for the average charge transition level $\epsilon^{2+/0}$ are compared in Table II and Fig. 4. In the GGA + U results, for defects with Ga-Ga, Ga-M, and M-M bonds, where M = In and Zn, the average transition levels are estimated to be 2.56, 2.12, and 2.14 eV above the VBM, respectively [Fig. 4(a)]. With the hybrid functional, the average transition levels are enhanced, whereas the average formation energies are reduced. In particular, the V_O defects with the Ga-Ga bonds exhibit a high transition level above the CBM. These defects may increase the carrier density, causing intrinsic n-type conductivity. However, their contribution will be very low because the defect concentration is low due to their high formation energies. For other defects with Ga-M and M-M bonds, the average transition levels are 2.98 and 3.05 eV,

TABLE II. The results of the GGA + U and hybrid density functional calculations are compared for the average charge transition levels ($\epsilon^{2+/0}$), the average formation energies (Ω), and the average defect levels (a_1) of V_O defects with Ga-Ga, Ga-M, and M-M bonds, which are denoted as V_O(Ga-Ga), V_O(Ga-M), and V_O(M-M), respectively. The $\epsilon^{2+/0}$ and a_1 levels are given with respect to the VBM and the formation energies are evaluated under the extreme O-rich condition.

	GGA + U			Hybrid density functional		
	V_O(Ga-Ga)	V_O(Ga-M)	V_O(M-M)	V_O(Ga-Ga)	V_O(Ga-M)	V_O(M-M)
$\Omega(V_O^0)$ (eV)	4.87	4.11	4.06	4.38	3.89	3.88
$\epsilon^{2+/0}$ (eV)	2.56	2.12	2.14	3.28	2.98	3.05
a_1 (eV)	0.86	0.94	1.09	1.35	1.38	1.64

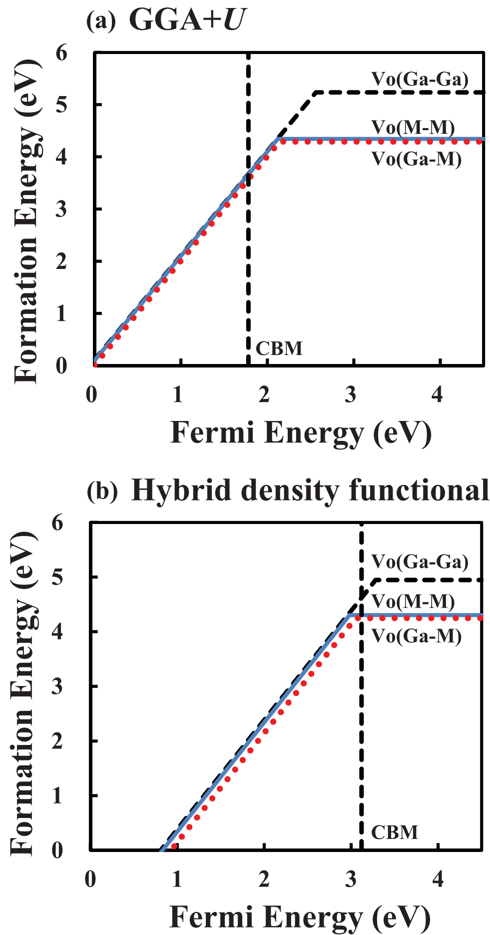

FIG. 4. (Color online) The average formation energies of V_O defects with Ga-Ga, Ga-M, and M-M bonds [V_O(Ga-Ga), V_O(Ga-M), and V_O(M-M), respectively] as functions of the Fermi energy for the neutral and +2 charge states in the (a) GGA + U and (b) hybrid density functional calculations.

respectively. As in the GGA + U results, the average transition levels are close to the CBM, because some of the defects have high transition levels, acting as shallow donors. Based on the GGA + U and hybrid density functional calculations, it is concluded that most V_O defects with low formation energies act as deep donors, while there are some shallow donors with high formation energies. The existence of shallow donors in a-IGZO results from the distinctive characteristics of the amorphous network, as compared to crystalline oxide semiconductors such as c-IGZO,[22] ZnO,[31,32,41] and SnO_2,[42] in which only deep donor levels were found.

In a-IGZO, the defect levels of V_O are also strongly affected by the local environment. Among 33 V_O defects considered, we find that 29 defects have deep defect levels in the band gap, which range from 0.61 to 1.52 eV above the VBM. These defect levels, which are distributed around the average value of 0.97 eV, are likely to correspond to the subgap states observed by x-ray photoemission spectroscopy measurements.[7] In the neutral charge state, as the metal atoms around the vacancy site undergo inward relaxations, strong interactions between the metal dangling bond orbitals result in the a_1 defect state in the band gap. The large lattice relaxations upon O-vacancy

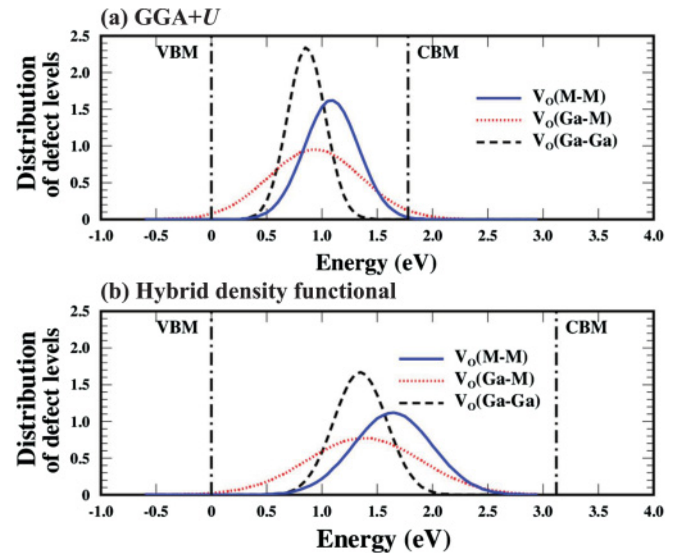

FIG. 5. (Color online) Comparison of the (a) GGA + U and (b) hybrid density functional calculations for V_O defects with Ga-Ga, Ga-M, and M-M bonds, for the distribution of the a_1 defect levels, in which peaks represent the average level positions.

formation reflect the covalent character of a-IGZO, as in ZnO.[43] For V_O defects with Ga-Ga, Ga-M, and M-M bonds, the average defect levels obtained by the GGA + U are positioned at 0.86, 0.94, and 1.09 eV, respectively, indicating that the defect levels are relatively low if Ga-Ga or Ga-M bonds are formed around the vacancy site [Table II and Fig. 5(a)]. In the hybrid functional calculations, the average defect levels shift to higher energies by about 0.5 eV, being mostly positioned deep in the band gap and keeping the same order in level position [Table II and Fig. 5(b)].

In c-IGZO with $m = 3$ [Fig. 1(b)], there exist four types of V_O defects, with the ratios of n_{In}:n_{Ga}:n_{Zn} = 3:0:1, 0:0:4, 0:1:3, and 0:3:0. In this case, V_O(0:0:4) is formed in the ZnO region, with four neighboring Zn atoms forming a tetrahedron, whereas V_O(0:3:0) has only Ga neighbors in the flat Ga-O layer. In previous GGA + U calculations,[22] all the defects were shown to exhibit inward relaxations and thereby have deep defect levels, with the lowest defect level for V_O(0:0:4). Similarly, in a-IGZO, the V_O(3:0:1), V_O(0:0:4), V_O(0:1:3), and V_O(0:3:0) defects are found to have deep defect levels at 1.06, 1.40, 0.93, and 0.90 eV above the VBM, respectively, although their defect concentrations are much lower than that of the V_O(1:1:1) defects, which have average defect level at 1.00 eV (Table III). In the case of V_O(0:0:4), because the neighboring Zn atoms are severely displaced from the tetrahedron, weak Zn-Zn interactions result in a high defect level.

In contrast to c-IGZO, there are exceptional V_O defects in a-IGZO, which exhibit shallow defect levels. Similar shallow defects were also found in previous local-density-functional approximation calculations for a-IGZO.[10] For four V_O defects, i.e., two V_O(1:1:1), one V_O(0:2:0), and one V_O(0:1:2) defects, the neighboring metal atoms undergo outward relaxations, as discussed earlier. In this case, the vacancy-neighboring atoms are strongly backbonded to the second-neighboring O atoms, and a void is created around the vacancy site. Due to weak interactions betwen the metal dangling bond orbitals, the a_1

TABLE III. The GGA + U calculations for the average defect levels (in units of eV) with respect to the VBM are compared for the $V_O(3:0:1)$, $V_O(0:0:4)$, $V_O(0:1:3)$, $V_O(0:3:0)$, and $V_O(1:1:1)$ defects in c- and a-IGZO. The results for c-IGZO are Ref. 22 and different defect levels result from different environments around the defects.

	$V_O(3:0:1)$	$V_O(0:0:4)$	$V_O(0:1:3)$	$V_O(0:3:0)$	$V_O(1:1:1)$
c-IGZO	1.4–1.5	1.1	1.4–1.5	1.4–1.5	
a-IGZO	1.06	1.40	0.93	0.90	1.00

defect state increases in energy, becoming a shallow level. As the defect level moves above the CBM, V_O is spontaneously ionized, with the ionized electrons in the CBM. In the hybrid functional calculations, the defect levels still lie above the CBM for three defects, while one of the $V_O(1:1:1)$ defects, which has the defect level close to the CBM in the GGA + U, becomes a deep donor when the band gap increases.

The defect levels of V_O play an important role in the stability of a-IGZO thin film transistors (TFTs) because V_O defects act as charge traps. In oxide TFTs under positive gate bias stress, positive shifts of V_{th} were observed.[6] Kamiya *et al.* suggested that there exist some V_O defects which create a second defect level near the CBM, so that even neutral defects can capture electrons, causing positive V_{th} shifts.[10] However, they did not consider the role of ionized V_O defects in device instability; these also cause the reduction of carrier concentrations. As ionized V_O defects can trap electrons, our result supplements the origin of positive V_{th} shifts observed under positive bias stress. Other defects, such as O_2 and H_2O molecules, which come from the ambient atmosphere, have also been suggested to be responsible for the positive V_{th} shift.[12,13]

On the other hand, when negative bias illumination stress is applied to a-IGZO TFTs, V_{th} exhibits large negative shifts up to −18 V. The NBIS instability was suggested to result from the trapping of photoinduced holes by defects,[20] especially V_O defects.[23] Under illumination of uv or visible light, electron-hole carriers are mostly generated in the channel material of a-IGZO, while the band gap of the dielectrics is much larger. As a negative bias voltage is applied, holes easily drift toward the interface, whereas electrons move away from the interface. Near the interface, neutral V_O defects are photoionized or capture drifting hole carriers, becoming V_O^{2+} defects. It was shown that the hole traps in a-IGZO are removed after a long time at room temperature, and the device stability is recovered rapidly by thermal annealing.[18,19] From these experiments, it is inferred that ionized V_O^{2+} defects recover the neutral charge state by capturing electrons, with various energy barriers which depend on the local bonding nature of V_O.

To examine the effect of thermal annealing on the recovery process, we perform molecular dynamics (MD) simulations within the GGA + U for the structural relaxation when V_O^{2+} captures two electrons. For six V_O defects, which have low, intermediate, and high charge transition levels (Table IV), we first optimize the geometries of V_O^{2+} using the conjugate gradient method at zero temperature. Outward relaxations of the neighboring metal atoms take place for all the ionized defects. When two electrons are captured, MD simulations for the recovery process are done for 8 ps at temperatures ranging from 200 to 400 °C. In c-IGZO, V_O defects are all deep donors,

TABLE IV. Thermal annealing effects are examined for six typical V_O defects, which have low, intermediate, and high transition levels ($\epsilon^{2+/0}$) in the initial configuration. The composition ratios (n_{In}:n_{Ga}:n_{Zn}) of the initial defects [$(V_O^0)_i$] are compared with those in the +2 charge state (V_O^{2+}) and in the final neutral configuration [$(V_O^0)_f$] after the MD simulations. In the last two columns, the defect levels (a_1) of $(V_O^0)_i$ and $(V_O^0)_f$ are given. In samples 2 and 4, the neutral state is not recovered, with the ionized electrons in the conduction band. The transition levels and defect levels relative to the VBM are obtained from the GGA + U calculations.

		n_{In}:n_{Ga}:n_{Zn}			a_1(eV)	
Sample	$\epsilon^{2+/0}$(eV)	$(V_O^0)_i$	V_O^{2+}	$(V_O^0)_f$	$(V_O^0)_i$	$(V_O^0)_f$
1	1.34	3:0:1	3:0:1	3:0:1	0.79	1.00
2	1.57	1:1:1	1:1:1	1:0:1	0.69	ionized
3	2.16	1:1:1	2:0:0	2:0:0	0.88	1.55
4	2.23	2:1:1	2:1:1	2:1:1	1.40	ionized
5	2.57	0:2:0	2:0:0	2:0:0	0.83	1.60
6	2.70	0:2:2	2:0:1	2:0:1	1.23	1.45

and ionized V_O^{2+} defects easily recover their original neutral configurations at zero temperature by capturing two electrons. Thus, there is no change in the total energy in c-IGZO, while the total energies in a-IGZO have a tendency to decrease in the final configurations of neutral V_O defects after MD simulations, compared with their initial neutral configurations.

Three distinct annealing effects were found in a-IGZO: structure recovery, reconstruction and diffusion, and shallow level formation.[23] In the structure recovery process, V_O^{2+} returns to the original defect at the same vacancy site after capturing two electrons, as in c-IGZO. For example, in the $V_O(3:0:1)$ defect (sample 1), which has a low transition level, relaxations of the neighboring metal atoms are found to be small in the +2 charge state. During the capture process, the ionized $V_O(3:0:1)^{2+}$ defect maintains the composition ratio of 3:0:1 and recovers the initial configuration at the same site even at room temperature. In the MD simulations at 400 °C, the defect site remains nearly unchanged, as shown in Fig. 6. The reconstruction-diffusion process occurs commonly for V_O defects with high transition levels (samples 3, 5, and 6). In the +2 charge state, reconstruction is significant in the amorphous network due to large outward relaxations around the vacancy site. We note that a second neighboring O atom fills in the vacancy site, and a different V_O defect is formed. As a consequence, V_O actually diffuses during the electron capture, especially toward an O site surrounded with In atoms. After the MD simulations at 200–300 °C, the ionized defects usually recover their neutral charge state by following the reconstruction-diffusion process. For the $V_O(0:2:2)$ defects (sample 6), which do not have In neighbors, we find that the final defect appears in the In-rich region, which is distant from the initial position by about 7 Å (Fig. 7). Finally, we address the fact that certain V_O^{2+} defects (samples 2 and 4) create a large void around the vacancy site, with the defect levels in the conduction band. In the electron capture process, these defects do not return to their original neutral state even at annealing temperatures of 500–600 °C, becoming shallow donors.

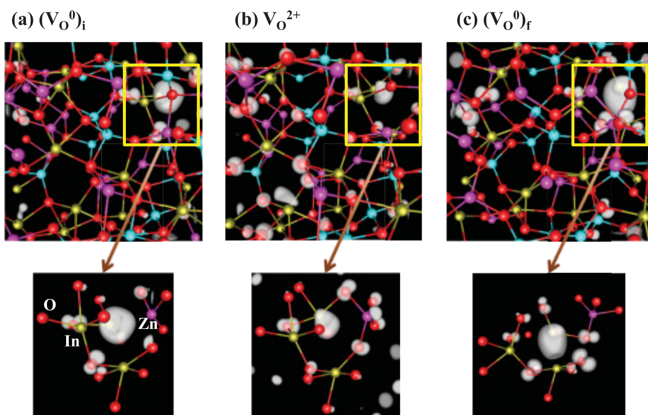

FIG. 6. (Color online) The atomic geometries for (a) the initial neutral $(V_O^0)_i$, (b) the ionized V_O^{2+}, and (c) the final neutral $(V_O^0)_f$ defect after molecular dynamics simulations at 400 °C in the structure recovery process of the original vacancy by electron capture. Isosurfaces of the charge densities are also shown for the defect level in each configuration.

Based on MD simulations at finite temperatures, we can classify ionized V_O^{2+} defects into two groups, which recover the neutral defect state at the same or different sites by capturing two electrons. While some defects easily capture electrons at room temperature, others need high annealing temperatures up to 400 °C to overcome the energy barrier between the ionized and neutral charge states. Under negative bias illumination stress, hole carriers drifting toward the interface can be captured by V_O defects near the interface, causing the negative shift of V_{th}. Our calculations show that hole traps can be removed by thermal annealing, recovering the device stability, in good agreement with experiments.[18,19] For a certain defect, the annealing temperature is found to be very high, above 600 °C, which is higher than the crystallization temperature. Considering the fact that the device stability is recovered at lower annealing temperatures, the high annealing temperature may result from the overestimation of the energy barrier for

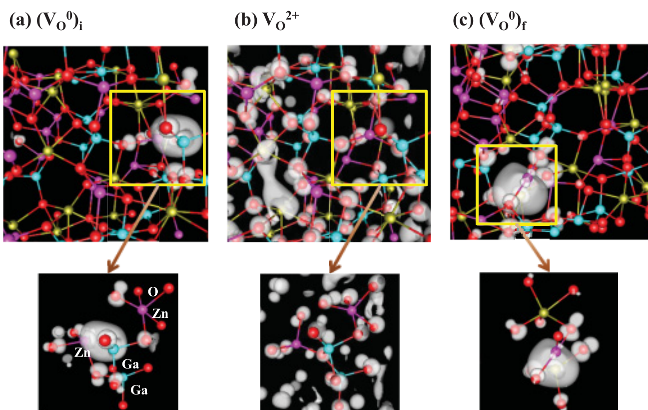

FIG. 7. (Color online) The atomic geometries for (a) the initial neutral $(V_O^0)_i$, (b) the ionized V_O^{2+}, and (c) the final neutral $(V_O^0)_f$ defect after molecular dynamics simulations at 200 °C in the reconstruction-diffusion process of the original vacancy by electron capture. Note that the vacancy site is displaced toward a different position. Isosurfaces of the charge densities are also shown for the defect level in each configuration.

the recovery of the neutral state by the GGA + U calculation. Due to the underestimation of the band gap, the energy of the ionized state with two electrons in the CBM is likely to be underestimated. At this point, it is difficult to do MD simulations within the hybrid density functional due to heavy computational demands. However, with inclusion of the band gap correction, as the energy barrier is lowered, the annealing temperature is expected to be reduced in MD simulations.

Finally, we discuss the role of impurities in device stability. It is known that hydrogen is a prevalent impurity in semiconductors and increases the n-type conductivity in SnO_2 and ZnO.[42,44] Similarly, in a-IGZO, the increase of n-type conductivity was observed in hydrogen-incorporated films.[45] In theoretical calculations, the enhanced n-type conductivity was attributed to interstitial hydrogen atoms which act as shallow donors.[46] As hydrogen may exist as a substitutional defect at the V_O site, this impurity will drastically change the role of V_O as a charge trap. However, it is not clearly resolved yet whether hydrogen incorporation improves NBIS instability or not. It was also reported that the device performance is very sensitive to ambient gases, such as O_2 and H_2O,[12,13] and to nitrogen incorporation.[47] Further studies are needed to investigate the role of hydrogen, nitrogen, and oxygen in the stability of a-IGZO devices.

IV. CONCLUSIONS

We have investigated the atomic and electronic properties of various V_O defects in a-IGZO using first-principles density functional calculations. We find that the formation energies of V_O have a tendency to increase with increasing number of neighboring Ga atoms. On the other hand, the formation energies are much reduced in the environment of In atoms, making it easy to generate O-deficient defects. As in c-IGZO, the CBM state is characterized by the In s orbital, insensitive to disorder, while the existence of distorted or undercoordinated O atoms induces localized states near the VBM. The results of calculations well explain the experimental findings that adding Ga atoms suppresses the instability of devices, whereas the carrier density and mobility are enhanced by increasing the In content. For neutral V_O defects, the neighboring metal atoms generally undergo inward relaxations, and the resulting interactions between the metal atoms give rise to deep donor levels in the band gap. While all V_O defects are deep donors in c-IGZO, there exist a few V_O defects in a-IGZO with shallow donor levels in the conduction band due to weak interactions between the metal atoms; these result from outward relaxations. It is suggested that shallow V_O defects are partly responsible for the positive V_{th} shift observed under positive gate bias stress. Under negative gate bias with light illumination stress, V_O defects in the channel material can be ionized, becoming V_O^{2+} defects due to the negative-U behavior. In this case, outward relaxations occur predominantly for the neighboring metal atoms. When two electrons are captured by applying a negative bias voltage, ionized V_O^{2+} defects return to the original neutral charge state. The recovery of neutral V_O defects occurs either at the initial sites or at different positions in the amorphous network, depending on the local environment. In addition, our molecular dynamics simulations show that although the recovery proceeds at

room temperature for some defects, other defects require high annealing temperatures up to 400 °C. Thus, the stability of devices is generally restored by annealing, in good agreement with experiments. Based on our calculations, we suggest that V_O defects play a role in the instability of *a*-IGZO-based thin film transistors.

ACKNOWLEDGMENTS

This work was supported by National Research Foundation of Korea (Grant No. NRF-2010-0093845) and the Information and Technology R&D program (Grant No. 2006-S079-02) of the Ministry of Knowledge Economy.

*kchang@kaist.ac.kr

[1] H. Q. Chiang, J. F. Wager, R. L. Hoffman, J. Jeong, and D. A. Keszler, Appl. Phys. Lett. **86**, 013503 (2005).
[2] K. Nomura, H. Ohta, A. Takagi, T. Kamiya, M. Hirano, and H. Hosono, Nature (London) **432**, 488 (2004).
[3] H. Yabuta, M. Sano, K. Abe, T. Aiba, T. Den, H. Kumomi, K. Nomura, T. Kamiya, and H. Hosono, Appl. Phys. Lett. **89**, 112123 (2006).
[4] D. Suresh, P. Wellenius, A. Dhawan, and J. F. Muth, Appl. Phys. Lett. **90**, 123512 (2007).
[5] A. Suresh and J. F. Muth, Appl. Phys. Lett. **92**, 033502 (2008).
[6] M. Kimura, T. Nakanishi, K. Nomura, T. Kamiya, and H. Hosono, Appl. Phys. Lett. **92**, 133512 (2008).
[7] K. Nomura, T. Kamiya, H. Yanagi, E. Ikenaga, K. Yang, K. Kobayashi, M. Hirano, and H. Hosono, Appl. Phys. Lett. **92**, 202117 (2008).
[8] M. Fuji, H. Yano, T. Hatayama, Y. Uraoka, T. Fuyuki, J. S. Jung, and J. Y. Kwon, Jpn. J. Appl. Phys. **47**, 6236 (2008).
[9] T. Kamiya, K. Nomura, M. Hirano, and H. Hosono, Phys. Status Solidi C **5**, 3098 (2008).
[10] T. Kamiya, K. Nomura, and H. Hosono, Phys. Status Solidi A **206**, 860 (2009).
[11] K. Takechi, M. Nakata, T. Eguchi, H. Yamaguchi, and S. Kaneko, Jpn. J. Appl. Phys. **48**, 011301 (2009).
[12] J. K. Jeong, H. W. Yang, J. H. Jeong, Y.-G. Mo, and H. D. Kim, Appl. Phys. Lett. **93**, 123508 (2008).
[13] M. E. Lopes, H. L. Gomes, M. C. R. Medeiros, P. Barquinha, L. Pereira, E. Fortunato, R. Martins, and I. Ferreira, Appl. Phys. Lett. **95**, 063502 (2009).
[14] Y.-K. Moon, S. Lee, W.-S. Kim, B.-W. Kang, C.-O. Jeong, D.-H. Lee, and J.-W. Park, Appl. Phys. Lett. **95**, 013507 (2009).
[15] J. Lee, J.-S. Park, Y. S. Pyo, D. B. Lee, E. H. Kim, D. Stryakhilev, T. W. Kim, D. U. Jin, and Y.-G. Mo, Appl. Phys. Lett. **95**, 123502 (2009).
[16] J.-M. Lee, I.-T. Cho, J.-H. Lee, W.-S. Cheong, C.-S. Hwang, and H.-I. Kwon, Appl. Phys. Lett. **95**, 222112 (2009).
[17] H. Hosono, K. Nomura, Y. Ogo, T. Uruga, and T. Kamiya, J. Non-Cryst. Solids **354**, 2796 (2008).
[18] K. Takechi, M. Nakata, T. Eguchi, H. Yamaguchi, and S. Kaneko, Jpn. J. Appl. Phys. **48**, 010203 (2009).
[19] T.-C. Fung, C.-S. Chuang, K. Nomura, H.-P. D. Shieh, H. Hosono, and J. Kanicki, J. Information Display **9**, 21 (2008).
[20] K.-H. Lee, J. S. Jung, K. S. Son, J. S. Park, T. S. Kim, R. Choi, J. K. Jeong, J.-Y. Kwon, B. Koo, and S. Lee, Appl. Phys. Lett. **95**, 232106 (2009).
[21] K. Nomura, T. Kamiya, H. Ohta, T. Uruga, M. Hirano, and H. Hosono, Phys. Rev. B **75**, 035212 (2007).
[22] W.-J. Lee, B. Ryu, and K. J. Chang, Physica B **404**, 4794 (2009).
[23] B. Ryu, H.-K. Noh, E.-A. Choi, and K. J. Chang, Appl. Phys. Lett. **97**, 022108 (2010).
[24] J. P. Perdew and Y. Wang, Phys. Rev. B **45**, 13244 (1992).
[25] P. E. Blöchl, Phys. Rev. B **50**, 17953 (1994).
[26] G. Kresse and J. Furthmüller, Phys. Rev. B **54**, 11169 (1996); G. Kresse and D. Joubert, *ibid.* **59**, 1758 (1999).
[27] X. Zhao, D. Ceresoli, and D. Vanderbilt, Phys. Rev. B **71**, 085107 (2005).
[28] S. Nosé, J. Chem. Phys. **81**, 511 (1984); Prog. Theor. Phys. Suppl. **103**, 1 (1991).
[29] N. Ashkenov, B. N. Mbenkum, C. Bundesmann, V. Riede, M. Lorenz, D. Spemann, E. M. Kaidashev, A. Kasic, M. Schubert, M. Grundmann, G. Wagner, H. Neumann, V. Darakchieva, H. Arwin, and B. Monemar, J. Appl. Phys. **93**, 126 (2003).
[30] S. L. Dudarev, G. A. Botton, S. Y. Savrasov, C. J. Humphreys, and A. P. Sutton, Phys. Rev. B **57**, 1505 (1998).
[31] A. Janotti and C. G. Van de Walle, Appl. Phys. Lett. **87**, 122102 (2005).
[32] A. Janotti and C. G. Van de Walle, Phys. Rev. B **76**, 165202 (2007).
[33] E. A. Albanesi, S. J. Sferco, I. Lefebvre, G. Allan, and G. Hollinger, Phys. Rev. B **46**, 13260 (1992).
[34] C. McGuinness, C. B. Stagarescu, P. J. Ryan, J. E. Downes, D. Fu, K. E. Smith, and R. G. Egdell, Phys. Rev. B **68**, 165104 (2003).
[35] J. P. Perdew, M. Ernzerhof, and K. Burke, J. Chem. Phys. **105**, 9982 (1996).
[36] C. G. Van de Walle and J. Neugebauer, J. Appl. Phys. **95**, 3851 (2004).
[37] W.-J. Lee, E.-A. Choi, J. Bang, B. Ryu, and K. J. Chang, Appl. Phys. Lett. **93**, 111901 (2008).
[38] W. K. Luo, H. W. Sheng, and E. Ma, Appl. Phys. Lett. **89**, 131927 (2006).
[39] D.-Y. Cho, J. Song, K. D. Na, C. S. Hwang, J. H. Jeong, J. K. Jeong, and Y.-G. Mo, Appl. Phys. Lett. **94**, 112112 (2009).
[40] S. Jeong, Y.-G. Ha, J. Moon, A. Facchetti, and T. J. Marks, Adv. Mater. **22**, 1346 (2010).
[41] S. J. Clark, J. Robertson, S. Lany, and A. Zunger, Phys. Rev. B **81**, 115311 (2010).
[42] A. K. Singh, A. Janotti, M. Scheffler, and C. G. Van de Walle, Phys. Rev. Lett. **101**, 055502 (2008).
[43] J. Carrasco, N. Lopez, and F. Illas, Phys. Rev. Lett. **93**, 225502 (2004).
[44] C. G. Van de Walle, Phys. Rev. Lett. **85**, 1012 (2000).
[45] A. Sato, K. Katsumi, R. Hayashi, H. Kumomi, K. Nomura, T. Kamiya, M. Hirano, and H. Hosono, Appl. Phys. Lett. **94**, 133502 (2009).
[46] T. Kamiya, K. Nomura, and H. Hosono, Phys. Status Solidi A **207**, 1698 (2010).
[47] P.-T. Liu, Y.-T. Chou, L.-F. Teng, F.-H. Li, and H.-P. Shieh, Appl. Phys. Lett. **98**, 052102 (2011).